



Thermo-capillary driven flow in macrolayer at high wall heat fluxes

Received October 1998
 Revised May 1999
 Accepted June 1999

Kuo-Tong Ma and Chin Pan

Department of Engineering and System Science, National Tsing Hua University, Hsinchu, Taiwan, Republic of China

Keywords *Flow, Macrolayer, Heat transfer*

Abstract *The present work is to investigate nucleate boiling heat transfer at high heat fluxes, which is characterized by the existence of macrolayer. Two-region equations are proposed to simulate both thermo-capillary driven flow in the liquid layer and heat conduction in the solid wall. The numerical simulation results can clearly describe the activities of several multi vortices in the macrolayer. These vortices and evaporation at the vapor-liquid interface constitute a very efficient heat transfer mechanism to explain the high heat transfer coefficient of nucleate boiling heat transfer near CHF. This study also explores the flow pattern of macrolayer with a high conducting solid wall, e.g. copper, and hence the temperature is uniform at the liquid-solid interface, and the heat fluxes and the evaporation coefficient are found to have significant effect on flow pattern in the liquid layer. Furthermore, a parameter "evaporation fraction" as well as "aspect ratio" is proposed as an index to investigate the thermo-capillary driven flow system. The model prediction agrees reasonably well with the experimental data in the literature.*

Nomenclature

A = area (m²)
 D_V = diameter of vapor stem (m)
 E = evaporation coefficient
 g = gravitational acceleration (ms⁻²)
 h_{evap} = evaporation heat transfer coefficient (Wm⁻²K⁻¹)
 h_{fg} = latent heat of vaporization (Jkg⁻¹)
 k = thermal conductivity (Wm⁻¹K⁻¹)
 M = molecular weight (kg kmole⁻¹)
 P = pressure (Nm⁻²)
 Pr = Prandtl number
 q''_w = heat flux (Wm⁻²)
 q = heat transfer rate (W)
 r = radial cylindrical coordinate (m)
 r_V = radius of vapor stem (m)
 r_L = radial distance from axis of symmetry to unit cell boundary (m)
 R = universal gas constant (J kmole⁻¹K⁻¹)
 T = temperature (K)
 v = velocity in radial direction (ms⁻¹)
 w = velocity in axial direction (ms⁻¹)
 z = axial cylindrical coordinate (m)

Greek symbols

β = volumetric thermal expansion coefficient (K⁻¹)
 δ = macrolayer thickness (m)
 δ_w = wall thickness (m)
 δ₂ = sum of macrolayer and wall thickness (m)
 μ = viscosity (kgm⁻¹s⁻¹)
 ρ = density (kgm⁻³)
 σ = surface tension (Nm⁻¹)
 ν_{fg} = difference of vapor and liquid specific volume (m³kg⁻¹)

Subscript

evap = evaporation
 ℓ = liquid
 stem = vapor stem interface
 sat = saturated
 v = vapor
 vapor = vapor interface (vapor stem interface + hovering bubble interface)
 w = wall

Introduction

Macrolayer has been found to play an important role in the prediction of near critical heat flux (CHF) heat transfer. It is presented as a thin liquid film between the heating surface and hovering bubbles that are nourished by the evaporation of vapor at the interface of the liquid film, i.e. the upper surface and the surface of vapor stem penetrating it (the vapor-liquid interface) as shown in Figure 1. The existence of the macrolayer is supported by the pool boiling experiments such as Gaertner and Westwater (1960), Gaertner (1965), Katto and Yokoya (1968), Bhat *et al.* (1986) and Shoji (1992), and by the flow boiling experiments such as Mudarwar and Maddox (1989). There are many different heat transfer models proposed in the literature regarding the evaporation of macrolayer. Gaertner (1965) postulated that the evaporation at the interface of the vapor-liquid is the major heat transfer mechanism of macrolayer. Katto and Yokoya (1968) and Yu and Mesler (1977) hypothesized that the evaporation of macrolayer is due to nucleate boiling. Bhat *et al.* (1986) resolved the heat transfer mechanism to the evaporation at the hovering bubble interface and the conduction through the macrolayer. Chyu (1987) attributed the evaporation of

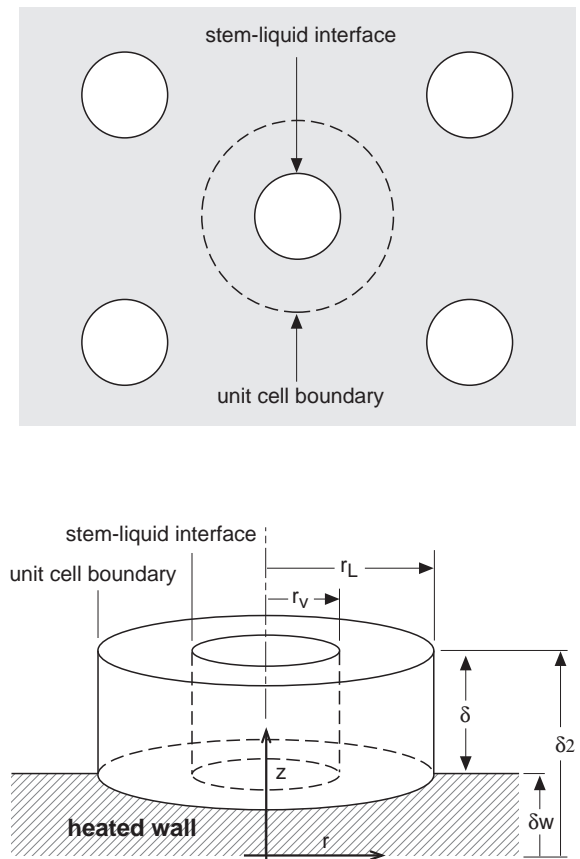


Figure 1.
Macrolayer, vapor stem,
hovering bubble and
interface

macrolayer to the microlayer, much thinner than macrolayer and existing on the bottom of vapor stem. Pan and Lin (1989) proposed that thermo-capillary driven flow and evaporation at the interface are the main heat transfer mechanisms for the macrolayer evaporation. Furthermore, Wang and Pan (1991) developed a mathematical model and carried out a numerical method to simulate the thermo-capillary driven flow in the macrolayer.

At the vapor-liquid interface, the surface tension gradient is produced by the temperature gradient formed during the heating process. Because the surface tension gradients create a discontinuity of the tangential shear stress at the vapor-liquid interface, both the liquid and vapor are driven to flow and such a flow is referred to as Marangoni flow in the literature. There have been many studies devoted to the effect of thermo-capillary driven flow on the nucleate flow boiling at low heat fluxes (Kao and Kenning, 1972; Gaddis, 1972; Kenning and Toral, 1977). However, there is lack of study devoted to thermo-capillary driven flow on the macrolayer at high heat fluxes, especially, by numerical method. Owing to numerical difficulties, only one case was studied by Wang and Pan (1991) that presents thermo-capillary driven flow pattern and non-uniform wall temperature distribution for water boiling at a heat flux of 900 kWm^{-2} under atmospheric condition.

The purpose of this study is to investigate thermo-capillary driven flow in the macrolayer for nucleate boiling at high flux by using the numerical method. The effect of a copper heated wall with a finite thickness is examined by a conjugated method coupling the region of liquid macrolayer and solid heated wall. Guglielmini and Nannei (1976) reported the significant effects of wall material on CHF for the distilled, degassed and saturated water at atmospheric pressure. They found that the CHF is asymptotically unchanged between the wall thickness from 10 to $50 \mu\text{m}$ for copper. Furthermore, the effect of evaporation coefficient, which has a certain degree of uncertainty (Kao and Kenning, 1972; Collier, 1972), for the interfacial heat transfer is also studied. The numerical results obtained in the present study will be compared with the experimental data to verify the effect of heat fluxes.

Mathematical model

The heat transfer mechanism of macrolayer is simulated by the thermo-capillary driven flow for nucleate boiling at high heat fluxes. A solid wall, existing between the macrolayer and the heating source, is also included to study the effect of heated wall. The following assumptions are made to simplify the analysis:

- The vapor stems are assumed to regularly distribute to the surface in the triangular lattice as shown in Figure 2a. A unit cell, with a central vapor stem is surrounded by an equivalent cylindrical liquid region (Figure 2b) in which the local transport of mass, momentum and heat are considered.
- The instantaneous macrolayer evaporation is simulated in the present study. Thus, the problem is simplified to be a steady state one, and only five variables P , V_ℓ , T_ℓ and T_S are solved. Since the time for

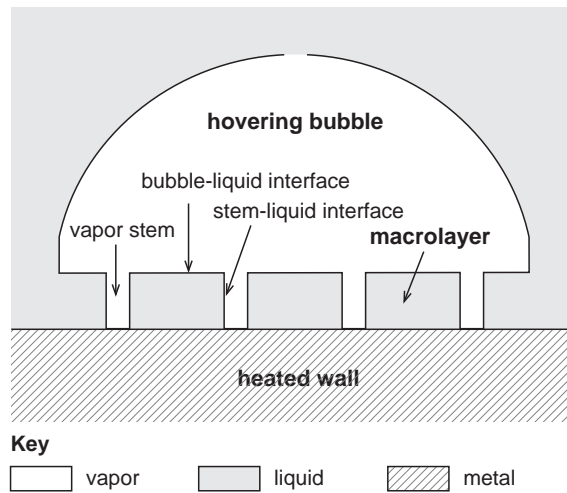


Figure 2.
(a) Regularly triangular
distribution of vapor
stems; (b) unit cell and
its relevant dimension

the evaporation of macrolayer is much longer than that for the thermo-capillary driven flow through the layer (Wang and Pan, 1991) (in the order of 10^3 from present calculation), it is reasonable to simulate the instantaneous heat transfer mechanism of macrolayer without the consideration of thickness reduction due to evaporation and to neglect the evaporation driven flow induced at the vapor-liquid interface.

- The buoyancy effect can be neglected for relatively thin macrolayer. Moreover, the numerical results confirm the assumption that the macrolayer is relatively thin and the Bond number, $-\frac{\rho_l g \beta \delta^2}{(\frac{\partial c}{\partial T})}$, is much smaller than 1 (Wang and Pan, 1991).
- The vapor temperature is set to be at the saturated state corresponding to system pressure. Because the density, thermal conductivity and viscosity of vapor are small as compared with liquid, the shear stress of vapor can be neglected in the hovering bubble and vapor stem penetrating the macrolayer. Therefore, the problem is further simplified to a two-region problem with the liquid macrolayer upon the solid wall.

Governing equations

Two-region (liquid layer and solid wall) equations are used to simulate the flow behaviors within the macrolayer. The governing equations are divided into two parts: one for the liquid flow in the macrolayer and the other for the solid wall.

(1) *Liquid:*

- Continuity equation:

$$\frac{1}{r} \frac{\partial(r \rho_\ell V_\ell)}{\partial r} + \frac{\partial(\rho_\ell w_\ell)}{\partial z} = 0 \quad (1)$$

- Axial momentum equation:

$$\frac{\partial(\rho_\ell v_\ell w_\ell)}{\partial r} + \frac{\partial(\rho_\ell w_\ell w_\ell)}{\partial z} = -\frac{\partial P}{\partial z} + \frac{1}{r} \frac{\partial}{\partial r} \left(r \mu_\ell \frac{\partial w_\ell}{\partial r} \right) + \frac{\partial}{\partial z} \left(\mu_\ell \frac{\partial w_\ell}{\partial z} \right) \quad (2)$$

- Radial momentum equation:

$$\frac{\partial(\rho_\ell v_\ell v_\ell)}{\partial r} + \frac{\partial(\rho_\ell w_\ell v_\ell)}{\partial z} = -\frac{\partial P}{\partial r} + \frac{1}{r} \frac{\partial}{\partial r} \left(r \mu_\ell \frac{\partial v_\ell}{\partial r} \right) + \frac{\partial}{\partial z} \left(\mu_\ell \frac{\partial v_\ell}{\partial z} \right) - \mu_\ell \frac{v_\ell}{r^2} \quad (3)$$

- Energy equation:

$$\frac{\partial(\rho_\ell v_\ell T_\ell)}{\partial r} + \frac{\partial(\rho_\ell w_\ell T_\ell)}{\partial z} = \frac{1}{r} \frac{\partial}{\partial r} \left(r \frac{\mu_\ell}{Pr} \frac{\partial T_\ell}{\partial r} \right) + \frac{\partial}{\partial z} \left(\frac{\mu_\ell}{Pr} \frac{\partial T_\ell}{\partial z} \right) \quad (4)$$

- (2) *Wall*. Energy equation:

$$\frac{1}{r} \frac{\partial}{\partial r} \left(r k_W \frac{\partial T_W}{\partial r} \right) + \frac{\partial}{\partial z} \left(k_W \frac{\partial T_W}{\partial z} \right) = 0 \quad (5)$$

Boundary conditions

At the stem-liquid interface. The presence of the surface tension gradient results in a discontinuity of the tangential shear stress at the interface. The shear stress due to possible vapor flow can be neglected without significant error because the vapor viscosity is much smaller than that of liquid. Thus,

$$-\mu_\ell \left(\frac{\partial w_\ell}{\partial r} + \frac{\partial v_\ell}{\partial z} \right)_{r=r_V} = \left(\frac{\partial \sigma}{\partial T_\ell} \right) \left(\frac{\partial T_\ell}{\partial z} \right) \Big|_{r=r_V} \quad (6)$$

The energy balance at the stem-liquid interface can be expressed as

$$k_\ell \left(\frac{\partial T_\ell}{\partial r} \right)_{r=r_V} = h_{evap} (T_\ell - T_{sat})_{r=r_V} \quad (7)$$

where h_{evap} is the heat transfer coefficient due to evaporation and can be approximated by the following equation (Pan *et al.*, 1986).

$$h_{evap} = \frac{2E}{2-E} \left(\frac{M}{2\pi R} \right)^{0.5} \frac{h_{fg}^2}{T_{sat}^{1.5} \nu_{fg}} \quad (8)$$

In the above equation, the evaporation coefficient E has the value varying from 0.03-0.05 (Collier, 1972; Hsu and Graham, 1986) to 1 (Kao and Kenning, 1972) for water. It is close to 1 for clean interface and is greatly decreased by

non-condensable gas and surface contamination at the interface (Kao and Kenning, 1972). Thermo-capillary driven flow

The liquid velocity induced by evaporation that is small compared with the thermo-capillary driven flow through the macrolayer can be neglect at the stem-liquid interface. Thus,

$$(v_\ell)_{r=r_V} = 0 \quad (9)$$

793

At the bubble-liquid interface. Following the similar arguments as at the stem-liquid interface, the boundary conditions at the bubble-liquid interface can be written as follows:

$$\mu_\ell \left(\frac{\partial w_\ell}{\partial r} + \frac{\partial v_\ell}{\partial z} \right)_{z=\delta_2} = \left(\frac{\partial \sigma}{\partial T_\ell} \right) \left(\frac{\partial T_\ell}{\partial r} \right) \Big|_{z=\delta_2} \quad (10)$$

$$k_\ell \left(\frac{\partial T_\ell}{\partial z} \right)_{z=\delta_2} = h_{evap} (T_\ell - T_{sat})_{z=\delta_2} \quad (11)$$

$$(w_\ell)_{z=\delta_2} = 0 \quad (12)$$

At the cell boundary. A symmetric boundary condition is applied to the unit cell boundary. Thus,

$$(v_\ell)_{r=r_L} = 0, \left(\frac{\partial w_\ell}{\partial r} \right)_{r=r_L} = 0, \left(\frac{\partial T_\ell}{\partial r} \right)_{r=r_L} = 0 \quad (13)$$

At the liquid-solid interface. The effective thermal conductivity deduced from conjugate heat transfer is used at the interface

$$k_{eff} = \frac{k_\ell k_W (\Delta z_W + \Delta z_\ell)}{(k_\ell \Delta z_W + k_W \Delta z_\ell)} \quad (14)$$

where Δz_ℓ and Δz_s represents the mesh size of liquid and solid neighboring the interface, and the no-slip condition is applied to the impermeable solid surface as

$$(v_\ell)_{z=\delta_W} = (w_\ell)_{z=\delta_W} = 0 \quad (15)$$

At outer surface of wall. A constant heat flux is imposed as the heat source at the outer surface of the wall

$$-k_W \left(\frac{\partial T_W}{\partial z} \right)_{z=0} = \frac{q''_W}{f} \quad (16)$$

where f is the fraction of the heating surface occupied by liquid. Since the vapor in stem has a comparatively small thermal conductivity, the imposed total heat

flux is assumed to be transferred through the liquid only. Consequently, the effective heat flux imposed at the wall is multiplied by the area correction factor, $1/f$.

Geometry setting

Gaertner (1965) measured the macrolayer thickness for saturated boiling of water at atmospheric pressure and gave the ratio of macrolayer thickness to vapor stem diameter as:

$$\delta = 0.6D_v = 1.2r_v \tag{17}$$

For a given heat flux and system pressure, Haramura and Katto (1983) postulated that the macrolayer thickness is one-fourth of the critical wavelength for Helmholtz instability. They then obtained the following equations for the initial macrolayer thickness and the fraction of the heating surface area.

$$\delta = 0.00536 \left(\frac{\rho_v}{\rho_\ell}\right)^{0.4} \left(1 + \frac{\rho_v}{\rho_\ell}\right) \sigma \rho_v \left(\frac{h_{fg}}{q''_W}\right)^2 \tag{18}$$

$$\frac{A_v}{A_L} = \left(\frac{r_v}{r_L}\right)^2 = 1 - f = 0.0654 \left[\left(\frac{11 \rho_\ell}{16 \rho_v} + 1\right)^{0.6} / \left(\frac{\rho_\ell}{\rho_v} + 1\right) \right]^{0.5} \tag{19}$$

These models are suitable for a vapor hovering bubble on the macrolayer growing relatively independent of the effect of previous detaching hovering bubble (Katto, 1992). Its hovering period is longer than the one under strong effect of (or penetrating into) the previous detaching hovering bubble, and the macrolayer thickness is comparatively thinner than some experimental data (Katto, 1992; Pasamehmetoglu and Nelson, 1987).

Table I lists the numerical values of macrolayer thickness, vapor stem and cell radii for water under atmospheric conditions at various heat fluxes from equations (17)-(19). From the experimental investigation of Guglielmini and Nannei (1976), the CHF for copper is asymptotically unchanged for the wall thickness from 10 to 50 μm. Thus, it is reasonable to select a value, 25 μm, to simulate the interaction between solid wall and liquid layer without the influence of wall thickness.

Table I.
Numerical values of associated geometry setting for various heat fluxes for water at atmospheric pressure

q''_W (Wm ⁻²)	6.0E5	6.75E5	7.5E5	8.25E5	9.0E5
δ (m)	1.374E-04	1.086E-04	80.800E-05	7.270E-05	6.109E-05
r_v (m)	1.145E-04	9.050E-05	7.335E-05	6.058E-05	5.091E-05
$r_L - r_v$ (m)	8.768E-04	6.928E-04	5.611E-04	4.637E-04	3.897E-04
$\frac{\delta}{r_L - r_v}$ (m)	0.157	0.157	0.157	0.157	0.157

Numerical treatment

The model developed in the previous section is solved numerically to investigate the flow behavior in the macrolayer. Differential equations describing the flow are made discrete by a finite difference approach. The hybrid scheme is used to treat the convective terms included in the governing equations, and the central difference scheme is employed for the diffusion terms. A well-known SIMPLE (Patankar, 1981) scheme is adopted to solve the coupled equations for the velocity and pressure. Throughout the steady-state calculation, the optimum false time given by the Courant criterion (Peyret and Taylor, 1983) is used to under-relax the calculation for velocities and temperature as

$$\Delta t_{false} = \frac{\Delta X}{U} = 1 \quad (20)$$

where ΔX is a characteristic length in the computation domain, U is a characteristic velocity.

The numerical procedure in solving this model is described as follows:

- (1) Set the boundary conditions (section 2.2) and the velocities inside the wall to be 0.
- (2) Solve the momentum equations for the velocities.
- (3) Solve the pressure correction equation based on the continuity equation to eliminate the mass conservation error.
- (4) Correct the velocities and update the pressure.
- (5) Solve the energy equations for the temperature.
- (6) Update the temperature relevant terms in boundary conditions: the surface tension gradients in equations (6) and (10), and evaporation heat sink in equations (7) and (11).
- (7) Repeat steps 2 through 6 until the convergent criteria are satisfied.

Several codes can be applied to solve this problem which include TEACH (Gosman and Ideriah, 1976), PHOENICS (CHAM, 1991), and FLOW3D (AEA, 1994) etc. The PHOENICS code is selected to solve this problem. A uniform-spaced grid system is used throughout the solution domain. Very fine grids are needed. Radial versus axial meshes, 215×90 , 270×110 and 325×130 (including 20 meshes for 25μ m copper wall), have been carried out to examine the grid independence. Temperature relevant terms in boundary conditions at the vapor-liquid interface are changed by the temperature distribution in the macrolayer until the steady convergence state is reached. The sensitivity studies on the grid systems show that the ratio of average temperature difference between two grid systems $< 10^{-4}$ is sufficient to capture the key phenomenon of heat transfer mechanism within the macrolayer. It needs 12,000 to 20,000 iterations for convergence.

Results and discussion

Present work intends to investigate thermo-capillary driven flow in the macrolayer for nucleate boiling at high flux with a copper heated wall. Two-region equations are applied to simulate the thermo-capillary driven flow in macrolayer with the interaction of the solid heated wall. The calculation results are compared with experimental data in the vapor mushroom region (Gaertner, 1965) that the complete macrolayer is formed under the hovering bubble.

Presence of copper wall

Figures 3(a) and 3(b) show the velocity vectors and temperature contours of thermo-capillary driven flow in the macrolayer above the solid wall (enveloped by a black box line). There are four vortex cells, which differ from five vortex cells reported by Wang and Pan (1991) without the consideration of the wall, generated in the macrolayer with the wall at the given heat flux $9E5 \text{ Wm}^{-2}$. The presence of the copper solid wall has a significant effect on the thermo-capillary driven flow in the macrolayer. In general, the temperature distribution of the liquid near the wall is much more uniform than that without considering the effect of wall. This could be verified by the maximum temperature difference 2°C shown in Figure 4 at the liquid-wall interface with wall, and 40°C (Wang and Pan, 1991) without wall respectively. A fairly uniform temperature distribution may explain why the number of vortex cells is reduced with the presence of the wall. Because the wall material, e.g. pure copper, has a very high thermal conductivity, the temperature near the heated wall is uniform. It induces a relatively high temperature gradient along the stem-liquid interface.

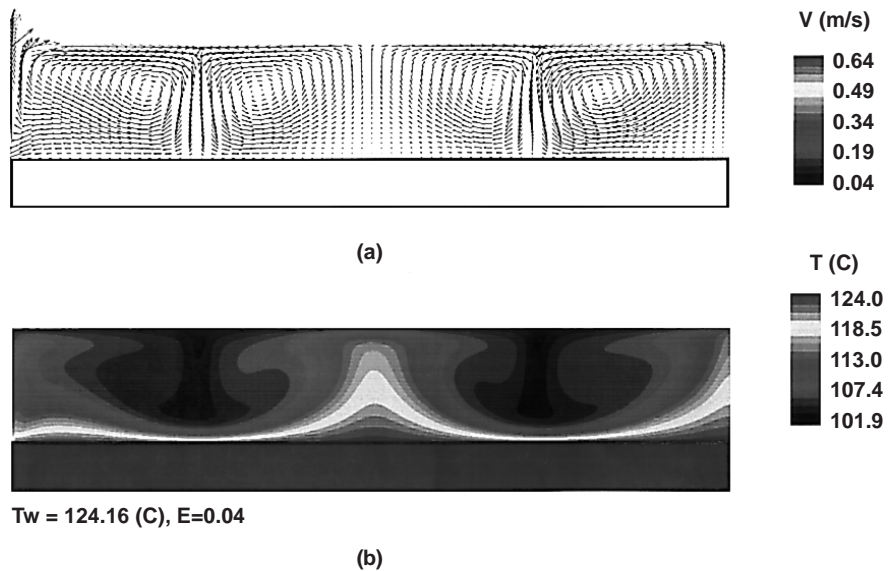


Figure 3.
Velocity vector and temperature contour for $q''_w = 9E5 \text{ Wm}^{-2}$

A colour version of this figure is available from the author

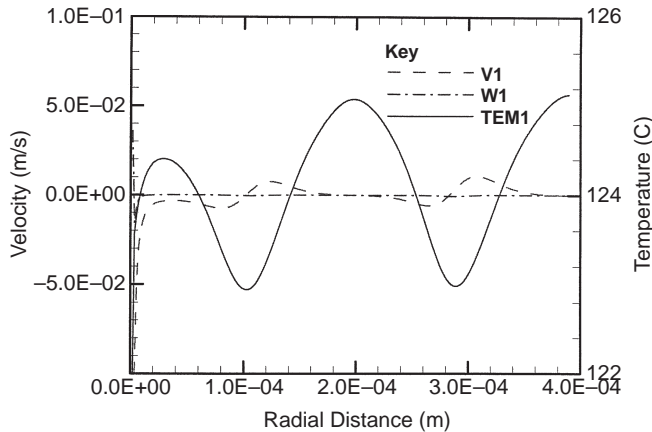


Figure 4. Velocity vector and temperature distributions at the liquid-wall interface for $q''_w = 9E5Wm^{-2}$

A stronger upward flow is generated at the stem-liquid interface and a much bigger clockwise vortex cell is formed near the vapor stem at the same time. That is the reason why the number of vortex cells reduces in the macrolayer in the presence of copper wall.

The velocity and temperature distribution in the macrolayer can be well explained by the simulation results as follows. In Figure 5, a negative temperature gradient is created along the stem-liquid interface as shown in the figure. This leads to a positive surface tension gradient along the stem-liquid interface to drive flow upward as the accelerated axial velocity W1. The upward flow is then hindered by the bubble-liquid interface and the residual fluid must move away from the interface. Therefore, a positive radial velocity is produced at the top of the layer. For the conservation of mass, a lateral flow is generated near the heating surface to compensate the upward mass flow and shown as a negative radial velocity V1. From the figure, it can also be noted that the lateral flow toward the stem-liquid interface is accelerated by the upward flow. The mass loss of the lateral flow is again compensated by the

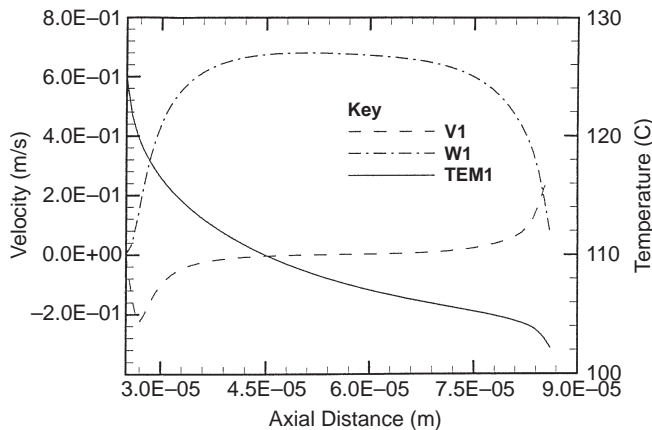


Figure 5. Velocity and temperature distributions at the stem-liquid interface for $q''_w = 9E5Wm^{-2}$

downward flow, which is an abruptly decelerated radial velocity induced at the bubble-liquid interface as shown in Figure 6. A clockwise vortex is, therefore, established by thermo-capillary driven flow near the stem-liquid interface as shown in Figures 3(a). This clockwise vortex will induce the subsequently sequential vortices with alternative direction in the radial and play an important role in constructing the vorticies.

The flow pattern in the temperature contour is depicted in Figure 3(b). A low temperature zone is created while the cooled liquid comes from the bubble-liquid interface impinging on the wall. On the other hand, a high temperature zone is formed while the liquid extracts heat energy from the wall and goes back to the interface. Figure 4 illustrates the impinging cooling of the cooler fluid driven by a pair of vorticies from the upper bubble-liquid interface, and the sinusoidal radial velocities produced within the temperature valleys. The cooler fluid is driven into and heated at the almost stagnant region where the liquid receives heat energy from the wall and produces a temperature peak there. It is seen that the heat energy transfer by the vorticies induced from thermo-capillary driven flow and evaporation at the vapor-liquid interface is a very efficient way.

Effect of heat fluxes

It would be interesting to examine the effect of heat fluxes of thermo-capillary driven flow in macrolayer. When the heat flux is decreased from $9E5 \text{ Wm}^{-2}$ to $6E5 \text{ Wm}^{-2}$, the macrolayer thickness, δ , vapor stem diameter, r_V , and the difference between cell outer diameter and vapor stem radius, $r_L - r_V$, as demonstrated in Table I are all increased by 2.25 folds except that the aspect ratio, $\delta/(r_L - r_V)$, remains unchanged. Both Figures 3(a) and 7(a) illustrate that there are four vortex cells created in the macrolayer at these two heat fluxes. This implies that the number of vortex cells produced in the macrolayer are related to the aspect ratio.

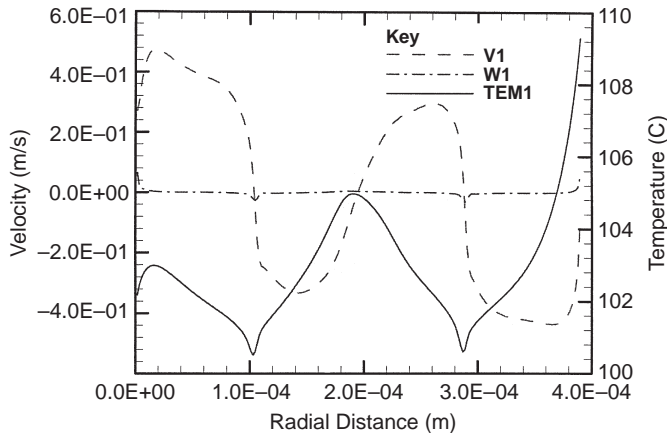
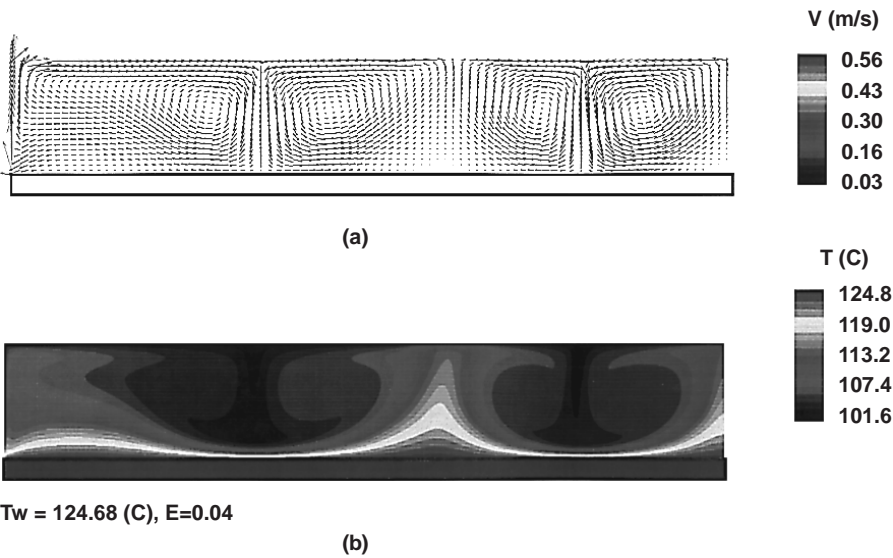


Figure 6. Velocity and temperature distributions at the bubble-liquid interface for $q''_w = 9E5 \text{ Wm}^{-2}$



Thermo-capillary
driven flow

Figure 7.
Velocity and vector and
temperature contour for
 $q''_w = 6E5Wm^{-2}$

A colour version of this figure is available from the author

Two different ways are coupled together to take the heated fluid energy away from macrolayer:

- (1) The vortex circulation, that mixed the cooler fluid from vapor-liquid interface with the warmer fluid from the heated wall inside the macrolayer.
- (2) The evaporation, that is able to cool the fluid at the vapor-liquid interface.

From the calculation results shown in Table II, about 90 per cent is taken away by evaporation at the bubble-liquid interface, and only a small portion (10 per cent) is transported from the stem-liquid interface. This stem-liquid interface takes only 3.25 per cent total area of the vapor-liquid interface. These results demonstrate that most of the heat energy diffused from the wall is removed from the macrolayer by evaporation at the bubble-liquid interface, while the evaporation per unit area at the stem-liquid interface is prior to the bubble-liquid interface. The heat transfer of clockwise vortex near vapor stem is more effective than that of the following alternative direction vorticities. It can be confirmed by the fact that the bubble-liquid interface, far from the heating surface, has a lower averaged temperature.

q''_w (Wm^{-2})	6.0E5	6.75E5	7.5E5	8.25E5	9.0E5
$\frac{q_{stem}}{q_{evapor}}$ (%)	10.38	10.18	9.25	8.72	8.57

Table II.
The evaporation
fraction for various
heat fluxes

Table II lists the numerical values of associated dimensionless parameter for heat flux. The evaporation fraction, the evaporation converted by the heat transfer rate from stem-liquid interface q_{stem} over that from vapor-liquid (stem-liquid and bubble-liquid) interface q_{vapor} , can be discriminated among the various heat fluxes. It can be seen that the evaporation fraction increased as the heat flux decreased. This is owing to the fact that the bubble-liquid interface is farther away from the heating surface as the macrolayer thickness increased, and the heat energy diffused from the stem-liquid interface more easily than from the bubble-liquid interface such that more heat energy is evaporated from the stem-liquid interface than from the bubble-liquid interface. Consequently, the clockwise vortex near the vapor stem is elongated to keep the balance of incoming (from liquid-solid interface) and outgoing (to vapor-liquid interface) heat energy in the macrolayer as the heat flux decreased. Comparing Figures 6 and 8, the results show that the regime of high temperature is diminished by the compressed vorticies of the subsequent alternative direction in the macrolayer and the evaporation is reduced at the bubble-liquid interface. Besides, the reduced temperature gradient for the increase of macrolayer thickness slows down the upward flow velocity along the stem-liquid interface, and provides less heat exchange rate (or evaporation) between the vapor and liquid interface as the coolant flow rate decreased in the heat exchanger. This decrease of evaporation for a reduced upward flow is against the increase of evaporation for the increased macrolayer thickness along the stem-liquid interface. However, it results in an increased evaporation at the stem-liquid interface as the heat flux decreased. This increased evaporation fraction varied the vortex pattern without change in the number of vortex cells in the macrolayer. The above evidence shows that the energy balance of the thermo-capillary driven flow system as well as the clockwise vortex near the vapor stem play the dominant role in the determination of the vortex pattern in the macrolayer.

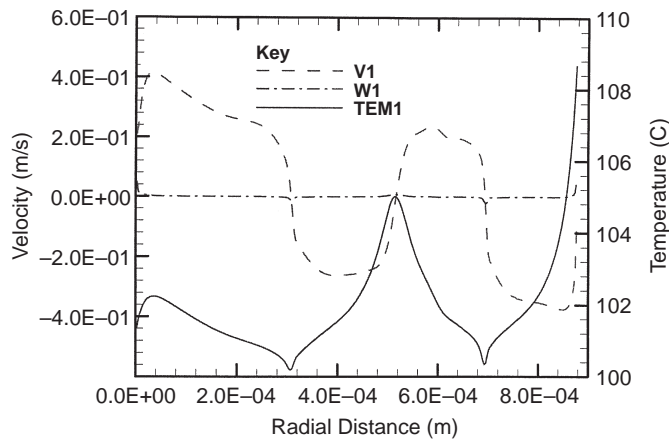


Figure 8.
Velocity and temperature distributions at the bubble-liquid interface for $q''_w = 6E5Wm^{-2}$

Constant temperature boundary

Since temperature variation is so small at the liquid-solid interface, the thermo-capillary driven flow is also calculated under a comparison condition that a constant temperature is given at the bottom boundary of the liquid layer without the consideration of high thermal conductivity wall. Under the heat flux $6E5Wm^{-2}$, an iteration of temperature is conducted for the constant temperature boundary to reach the heat flux. Comparing with Figures 7 and 9, we can see that the velocity vectors and temperature contours of those two conditions are quite similar to each other. It illustrates the consistency of the present study that the macrolayer with the high thermal conductivity wall could be approximately simulated by the constant temperature boundary approach. Nevertheless, the temperature of the constant temperature boundary, $122.5^{\circ}C$, is smaller than that with the wall ($124.68^{\circ}C$) under the same heat flux. The average heat transfer coefficient would be larger under constant temperature boundary condition.

Effect of evaporation coefficient

As mentioned previously, there is a certain degree of uncertainty for the evaporation coefficient E . A sensitivity study of the evaporation coefficient is, therefore, applied to evaluate the effect of evaporation coefficient on the thermo-capillary driven flow in the macrolayer. Figure 10 demonstrates that evaporation fraction is increased with the increase of evaporation coefficient. The results describe the evaporation coefficient E varied from 0.03 to 0.08 at heat flux $6E5Wm^{-2}$, and the heat transfer coefficient h_{evap} , varied from 0.746 to 2.042 based on the heat transfer coefficient at $E = 0.04$. Because the stem-liquid interface is

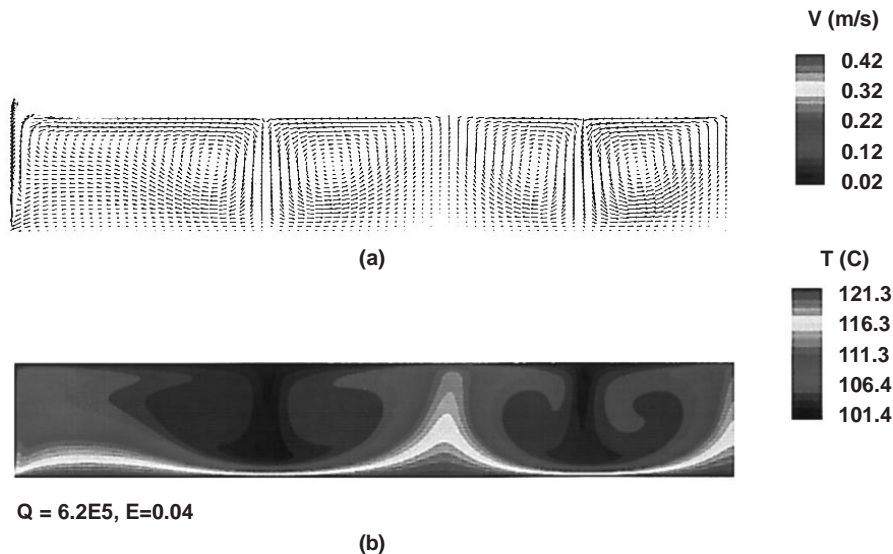


Figure 9.
Velocity vector and
temperature contour for
constant temperature
boundary

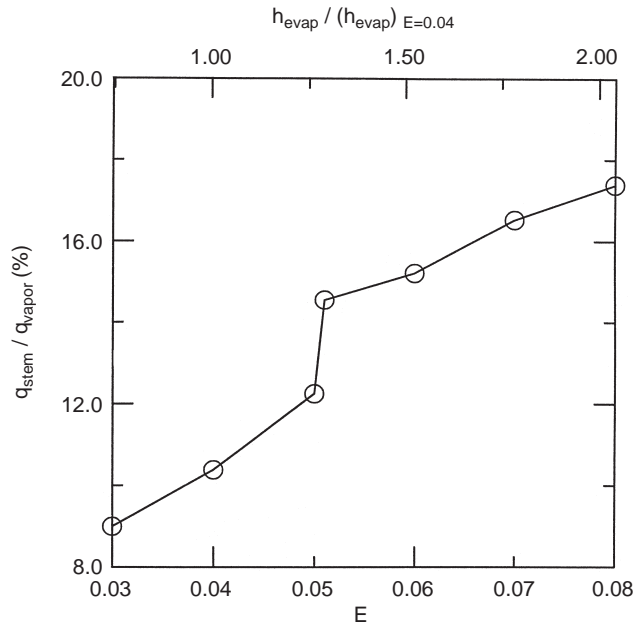


Figure 10.
Evaporation fraction
distribution versus
evaporation coefficient
for $q''_w = 6E5Wm^{-2}$

near the heating surface, the heat energy released from the stem-liquid interface is easier than from the bubble-liquid interface by the increased evaporation coefficient (or the increased heat sink). Although the stem-liquid interface has the same evaporation coefficient as the bubble-liquid interface, the stem-liquid interface obtains more heat energy to evaporate than bubble-liquid interface.

Figure 11 shows a sharp averaged wall temperature increment as E slightly increased from 0.05 to 0.051, but has a small increment for $E \leq 0.05$ and $E \geq 0.051$. There is a significant change in macrolayer flow pattern for $E > 0.05$ that the number of vortex cells in the macrolayer is decreased from four to three as shown in Figure 12. Because the enhanced evaporation at the stem-liquid interface for high evaporation coefficient attracts more liquid towards the interface to compensate the additional mass loss, and a stronger clockwise vortex near the vapor stem is then produced. More heat energy would be collected by this vortex from the heating surface and taken away by the evaporation at the stem-liquid interface. On the other hand, the four vortex cells within the macrolayer are not able to afford further work to decrease the evaporation at the bubble-liquid interface as $E > 0.05$, the thermo-capillary driven flow system adjusts the vortex pattern by reducing the number of vortex cells to keep the energy balance. However, the reduction of vortex cells in the macrolayer also implies that the heating surface has lower impingement cooling by the cooler fluid driven by vortex cells. Therefore, there is a sharp increase in the average wall temperature as E slightly increased from 0.05 to 0.051. This sharp change is due to the energy balance of system affected by the evaporation fraction that may be slightly dependent on system. As the results proposed by

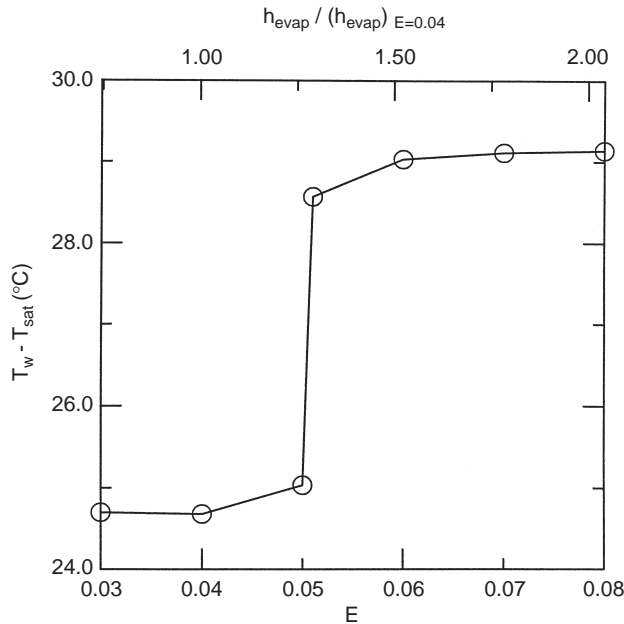


Figure 11.
Average wall
temperature distribution
versus evaporation
coefficient for $q_w'' =$
 $6E5Wm^{-2}$

Wang and Pan (1991), the evaporation coefficient $E = 0.04$ is a quite reasonable value to achieve the wall with relatively low averaged temperature; that is, a higher heat transfer coefficient is obtained by $E = 0.04$. In the circumstance, the vortex pattern has the capability to bring heat energy effectively from the heated wall and then evaporate at the vapor-liquid interface.

Comparison with experimental data

The calculated value agrees reasonably well with both the experimental data of Gaertner (1965) and Nishikawa *et al.* (1984) as shown in Figure 13. The over-prediction of averaged wall temperature may be caused by the relatively thick macrolayer and large cell width based on the model of Haramura and Katto (1983). Moreover, the macrolayer thickness and/or cell width must be reducing by the evaporation at the vapor-liquid interface. The present model using initial macrolayer thickness and cell width may be unrealistic for the macrolayer evaporation process. By comparing Figure 14(a) with Figure 7(b), it can be noted that the number of vortex cells in the macrolayer keeps unchanged for the same aspect ratio. However, the number of vortex cells will change with the aspect ratio as demonstrated in Figure 14(b) and 14(c) for half width and half thickness of the macrolayer, respectively. Experimental observation of Villers and Platten (1992) also illustrates the effect of the aspect ratio on the number of vortex cells. Besides the aspect ratio, this study also extends the change of vortex pattern to the evaporation fraction as illustrated in Table III. The larger the evaporation fraction, the less the number of vortex cells or the bigger the clockwise vortex cell near the vapor stem. This has been proven in the previous

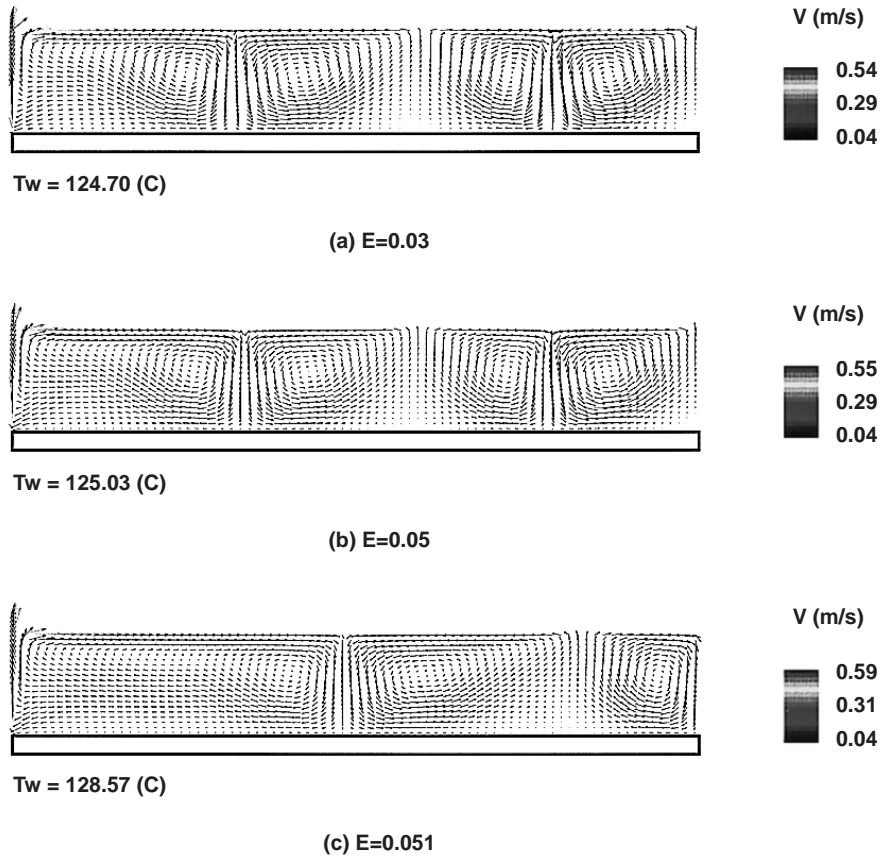


Figure 12. Comparison of velocity vectors for (a) evaporation coefficient $E = 0.03$; (b) evaporation coefficient $E = 0.05$; (c) evaporation coefficient $E = 0.051$ at $q''_w = 6E5Wm^{-2}$

A colour version of this figure is available from the author

section. Moreover, the averaged wall temperature decreased obviously when the thickness and width are reduced to a half, and the calculated results obtained for experimental data is thus much better as shown in Figure 13. Therefore, it is essential to evaluate the experimental wall temperature, which is averaged from the macrolayer evaporation process, while comparing the simulation results with the experimental data.

Conclusions

The purpose of this study is to develop a numerical approach to simulate flow behaviors and heat transfer for nucleate boiling of water at high heat fluxes from two-region equations. The flow behaviors in the macrolayer, such as the interaction between the liquid layer and solid wall, the effect of heat fluxes and the evaporation coefficient, are investigated. On nucleate boiling curve, the model predictions at high heat flux are in reasonably good agreement with

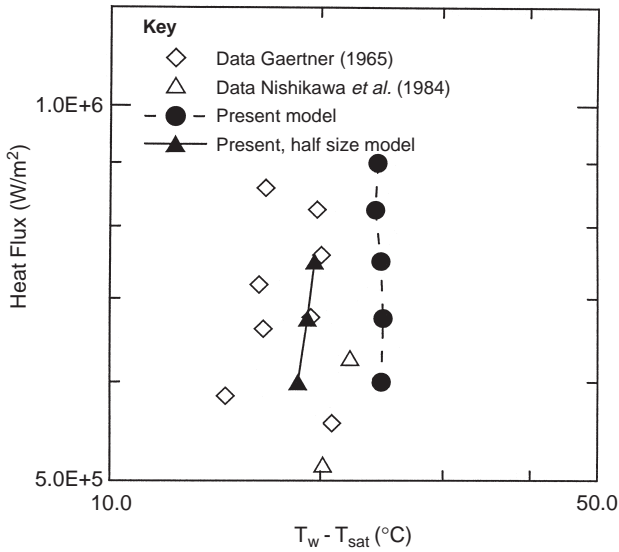


Figure 13. Comparison of the present calculation with the experimental data for $q''_w = 6E5Wm^{-2}$

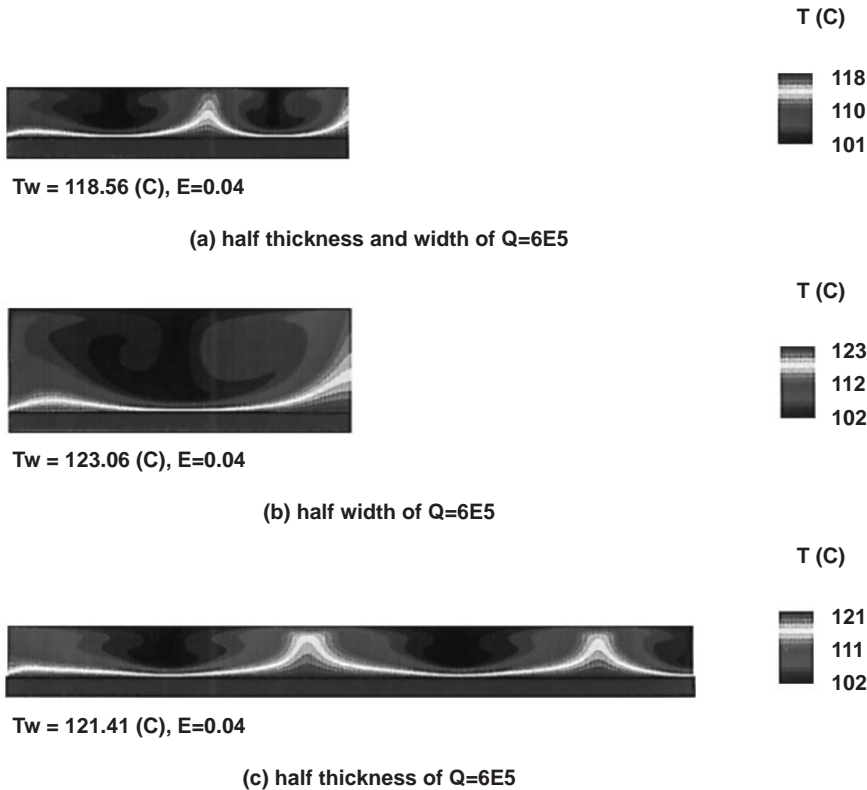


Figure 14. Comparison of temperature contour for (a) half thickness and cell width; (b) half cell width; (c) half thickness of the macrolayer at $q''_w = 6E5Wm^{-2}$

A colour version of this figure is available from the author

experimental data in the literature. The following conclusions may be obtained from the present study:

- With the thermo-capillary driven flow, the vortex cells are induced in the vapor-liquid interface of the macrolayer, at which the heat energy can be efficiently carried away from the heated wall by the vortex cells and the evaporation. These vortex cells and evaporation at the vapor-liquid interface constitute a very efficient heat transfer mechanism to explain the high heat transfer efficiency of the nucleate boiling heat transfer near CHF.
- The temperature distribution along the liquid-solid interface is uniform because of high conductivity solid wall. It produces a big and strong clockwise vortex cell near the vapor stem and reduces the total number of vortex cells in the presence of wall. Furthermore, the flow pattern and temperature contours are quite the same as those of a wall with constant temperature.
- The major part (~90 per cent) of the heat energy diffused from the heating surface is taken away by the evaporation at the bubble-liquid interface. However, the evaporation per unit area at the stem-liquid interface is much better than that of the bubble-liquid interface. A parameter “evaporation fraction” as well as “aspect ratio” can be applied as an index to investigate the thermo-capillary driven flow system.
- As the heat flux decreased, the clockwise vortex near the vapor stem is elongated to keep the energy balance in the macrolayer for the increased evaporation fraction. The energy balance in addition to the clockwise vortex near the vapor stem play a dominant role to determine the vortex pattern in the thermo-capillary driven flow system.
- In case of evaporation coefficient $E = 0.04$ for water, a common value used in the literature, the relative low averaged wall temperature can be achieved by the vortex pattern. That is because the heat energy can effectively take away from the heated wall and evaporate at the bubble-liquid interface. It can be noted that the evaporation fraction increases while the evaporation coefficient increases. Especially, there exists an abruptly step rise in the evaporation fraction and the averaged wall temperature distribution when the evaporation coefficient is increased from 0.05 to 0.051. The number of vortex cells is reduced as the evaporation coefficient $E > 0.05$.
- The number of vortex cells is changed with the aspect ratio. On the other hand, the number of vortex cells remains unchanged if both thickness

Table III.
The evaporation fraction for associated dimension at $q''_w = 6E5Wm^{-2}$

	δ	0.5δ	$0.5 (r_L - r_v)$	0.5δ and $0.5 (r_L - r_v)$
$\frac{q_{stem}}{q_{vapor}}$ (%)	10.38	6.91	24.71	8.57

and cell width of the macrolayer are varied to keep the aspect ratio unchanged. Moreover, the increase of the evaporation fraction will alter the vortex pattern in the macrolayer without change in the number of vortex cells.

References

- AEA (1994), *CFDS-FLOW3D Release 3.3: USER MANUAL*, Computational Fluid Dynamics Services, AEA Technology.
- Bhat, A.M., Saini, J.S. and Prakash, P. (1986), "Role of macrolayer evaporation in pool boiling at high heat flux", *Int. J. Heat Mass Transfer*, Vol. 29 No. 12, pp. 1953-61.
- CHAM (1991), *The PHOENICS Beginner's Guide*, CHAM/TR100, Concentration Heat and Momentum Limited.
- Chyu, M.C. (1987), "Evaporation of macrolayer in nucleate boiling near burnout", *Int. J. Heat Mass Transfer*, Vol. 30 No. 7, pp. 1531-8.
- Collier, J.G. (1972), *Convective Boiling and Condensation*, 2nd ed., McGraw-Hill, New York, NY, p. 322.
- Gaddis, E.S. (1972), "The effects of liquid motion induced by phase change and thermocapillarity on the thermal equilibrium of vapor bubble", *Int. J. Heat Mass Transfer*, Vol. 15, pp. 2241-50.
- Gaertner, R.F. (1965), "Photographic study of nucleate pool boiling on a horizontal surface", *J. Heat Transfer*, Vol. 87, pp. 17-29.
- Gaertner, R.F. and Westwater, J.W. (1960), "Population of active sites in nucleate boiling heat transfer", *Chem. Eng. Progress Symp. Series*, Vol. 56, pp. 39-48.
- Gosman, A.D. and Ideriah, P.J.K.I. (1976), *TEACH-2E: A General Computer Program for Two-dimensional, Turbulent, Recirculating Flow*, Department of Mechanical Engineering, Imperial College, London.
- Guglielmini, G. and Nannei, E. (1976), "On the effect of heating wall thickness on pool boiling burnout", *Int. J. Heat Mass Transfer*, Vol. 19, pp. 1073-5.
- Haramura, Y. and Katto, Y. (1983), "A new hydraulic model for critical heat flux, applicable widely to both pool and forced convection boiling on submerged bodies in saturated liquids", *Int. J. Heat Mass Transfer*, Vol. 26, pp. 389-99.
- Hsu, Y.Y. and Graham, R.W. (1986), *Transport Processes in Boiling and Two-Phase Systems Including Near-critical Fluids*, American Nuclear Society, La Grange Park, IL, pp. 55-8.
- Kao, Y.S. and Kenning, D.B.R. (1972), "Thermocapillary flow near a hemispherical bubble on a heated wall", *J. Fluid Mech.*, Vol. 53 No. 4, pp. 715-35.
- Katto, Y. and Yokoya, S. (1968), "Principle mechanisms of boiling crisis in pool boiling", *Int. J. Heat Mass Transfer*, Vol. 11, pp. 993-1002.
- Katto, Y. (1992), "Critical heat flux in pool boiling", *Engineering Foundation Conf., Pool and External Flow Boiling*, Santa Barbara, CA, 22-27 March, pp. 151-64.
- Kenning, D.B.R. and Toral, H. (1977), "On the assessment of thermocapillary effects in nucleate boiling of pure fluids", *Int. Conf. Phys. Chem. and Hydrodynamics*, (Levich Birthday Conf.), Oxford.
- Mudarwar, I. and Maddox, D.E. (1989), "Critical heat flux in subcooled flow boiling of fluorocarbon liquid on a simulated electronic chip in a vertical rectangular channel", *Int. J. Heat Mass Transfer*, Vol. 32 No. 2, pp. 379-94.
- Nishikawa, K., Fujita, Y., Uchida, S. and Ohta, H. (1984), "Effect of surface configuration on nucleate boiling heat transfer", *Int. J. Heat Mass Transfer*, Vol. 27, pp. 1559-71.

-
- Pan, C. and Lin, T.L. (1989), "Marangoni flow on pool boiling near critical heat flux", *Int. Comm. Heat Mass Transfer*, Vol. 16, pp. 475-86.
- Pan, C., Jones, B.G. and Machiels, A.J. (1986), "A combined heat and solute transport model in porous deposits with chimney", *Proc. of the 8th Int. Heat Transfer Conf.*, San Francisco, CA, pp. 2117-22.
- Pasamehmetoglu, K.O. and Nelson, R.A. (1987), "The effect of Helmholtz instability on the macrolayer thickness in vapor mushroom region of nucleate pool boiling", *Int. Comm. Heat Mass Transfer*, Vol. 14, pp. 709-20.
- Patankar, S.V. (1981), *Numerical Heat Transfer and Fluid Flow*, Hemisphere, Washington, DC.
- Peyret, R. and Taylor, T.D. (1983), *Computational Methods for Fluid Flow*, Springer Series in Computational Physics, Springer-Verlag, Berlin.
- Shoji, M. (1992), "A study of steady transition boiling of water", *Engineering Foundation Conf., Pool and External Flow Boiling*, Santa Barbara, CA, 22-27 March, pp. 237-42.
- Villers, D. and Platten, J.K. (1992), "Coupled buoyancy and Marangoni convection in acetone: experiments and comparison with numerical simulations", *J. Fluid Mech.*, Vol. 234, pp. 487-510.
- Wang, F.M. and Pan, C. (1991), "Thermocapillary driven flow in the macrolayer for nucleate boiling at high heat fluxes", *Proc. of the 4th Int. Symp. on Transport Phenomena in Heat and Mass Transfer*, Sydney, Australia, 14-19 July, Vol. 1, pp. 550-61.
- Yu, C.L. and Mesler, R.B. (1977), "A study of nucleate boiling near the peak heat flux through measurement of transient surface temperature", *Int. J. Heat Mass Transfer*, Vol. 20, pp. 827-40.